2021 43rd Annual International Conference of the
IEEE Engineering in Medicine & Biology Society (EMBC)
Oct 31 - Nov 4, 2021. Virtual Conference

Practical Implementation of a Novel Output Impedance Measurement Technique for EIT System While Attached to a Load*

Omid Rajabi Shishvan[1], Ahmed Abdelwahab[1], and Gary J. Saulnier[1]

***Abstract*— A novel method for measuring the output impedance of current sources in an EIT system is implemented and tested. The paper shows that the proposed method can be used at the time of operation while the load is attached to the EIT system. the results also show that performance of the system improves when the shunt impedance values from the proposed technique are used to set the adaptive sources as opposed to the shunt impedance values acquired through open circuit measurements.**

I. Introduction

Electrical Impedance Tomography (EIT) is an imaging method that generates a map of the internal impedance distribution of an object. EIT can be used on humans to map the internal organs, especially the thorax where the lungs inflate and deflate with high impedance air and the heart pumps low impedance blood through the body. EIT functions by applying electrical currents to the subject through surface-mounted electrodes and measuring the induced voltages on those electrodes. These voltages are then used to construct the impedance map of the internal organs by solving the mathematical inverse problem. EIT systems typically employ current sources to apply the currents.

One disadvantage of the EIT systems is that the inverse problem is ill-posed [1], meaning that small errors in the operation of the systems might translate into considerable artifacts in reconstructed images. One source of such errors can be attributed to the shunt impedance that is present at the output of current sources. EIT systems need to apply precise currents and the existence of this shunt impedance in parallel to the subject of imaging results in some of the current being lost and not delivered to the subject, introducing inaccuracies. Compensating for the lost current in the shunt impedance dampens its effects on the final images.

A novel technique for measuring the shunt impedance of current sources was introduced in [2]. This paper implements the proposed idea from [2] on a multiple-source EIT system with 32 adaptive current sources [3], [4] to demonstrate both the feasibility and accuracy of the proposed method. The current sources use an estimate of the shunt impedance, including that introduced by cabling, to supply the additional current needed to compensate for the losses in that impedance. The result is that the desired current is supplied to the load. The combination of this current source and the method introduced in [2] enables the shunt impedance to be continuously estimated and updated while the system is performing its imaging operation. Being able to update the output impedance values while imaging not only simplifies the calibration procedure by eliminating the need to disconnect the sources from the patient to obtain the shunt impedance values but also makes it possible to maintain accuracy in a long-term monitoring application.

The paper is organized as follows: Section II presents properties of an EIT system. Section III goes over the impedance measurement model. The experimental setup and the experiments are discussed in Section IV. Section V depicts the results and Section VI provides the conclusion and a roadwork to the future work.

II. EIT Systems

To take an image, an EIT system applies electrical current through the electrodes attached around the periphery of an object. The induced voltages on the electrodes are then taken and turned into an image of the impedance distribution of the interior of the object. Although EIT systems can operate with only one or two current sources that are connected to the electrodes through a multiplexer [5], the EIT system considered in this paper is a multiple-source system where every electrode has a dedicated current source. All of these electrodes are simultaneously injecting current into the body. A simplified depiction of an EIT system with only 4 electrodes and 4 sources is shown in Fig. 1. The sources apply currents which ideally sum up to zero, but the existence of finite output impedance in parallel with the current sources causes the current injected into the body to differ from the current generated by the source on each electrode. For this reason, an extra electrode connects the body to a ground or virtual ground node where the current mismatch is drained. For the system considered in this paper, this mismatch current is also measured at the time of operation.

A. Standard Current Patterns

The applied currents are sinusoids where their amplitude and phase follows certain constraints. One of the main constraints is that the sum of the injected currents should equal zero. Additionally, for a given amount of resources, the applied currents should provide the maximum possible amount of information to the reconstruction algorithm, leading to the use of orthogonal current patterns where a pattern defines the current for each electrode. A set of trigonometric

*Research reported in this paper was supported by the National Institute of Biomedical Imaging and Bioengineering of the National Institutes of Health under award number 1R01EB026710-01A1. The content is solely the responsibility of the authors and does not necessarily represent the official views of the National Institutes of Health.

[1]O. Rajabi Shishvan, A. Abdelwahab, and G J. Saulnier are with Electrical and Computer Engineering Department, University at Albany - State University of New York, Albany, NY, USA {orajabishishvan, aabdelwahab, gsaulnier}@albany.edu

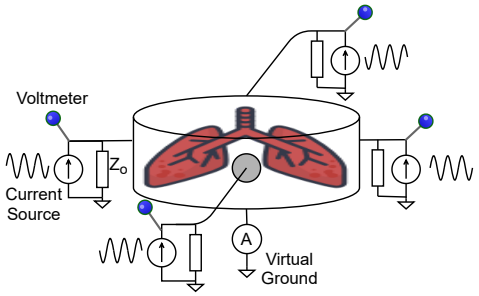

Fig. 1: A Simplified EIT system with 4 sources, applying current simultaneously to the body and measuring the voltage on the electrodes. Each source has a parallel impedance and the body is connected to virtual ground using an additional electrode to address any current injection mismatch.

current patterns are generally used for two dimensional imaging in multiple source systems [6] with N electrodes as shown in (1)

$$I_{S_j}^i = \cos\left(\frac{2\pi * j * i}{N}\right) \text{ for } 1 \le j \le N, 1 \le i \le \frac{N}{2}$$
$$I_{S_j}^{i+\frac{N}{2}} = \sin\left(\frac{2\pi * j * i}{N}\right) \text{ for } 1 \le j \le N, 1 \le i < \frac{N}{2} \quad (1)$$

where $I_{S_j}^i$ is the amplitude of current from the jth source in ith pattern. For a system with N electrodes, (1) defines a set of $N-1$ patterns that are orthogonal to each other and individually sum up to zero. These trigonometric patterns are optimal for a circular region of homogeneous conductivity.

B. Parallel Output Impedance Estimation

The standard current patterns are developed under the assumption that they are delivered to the body without any loss. In practice, current intended for the load is shared with the parallel output impedance of sources. Various output impedance measurement techniques have been proposed in the literature and used with calibration techniques to reduce the current loss and resulting degradation of the data. The authors in [7] introduced using a resistive droop measurement to calculate the output impedance. In this technique two known resistive loads are sequentially attached to the output of the current source when applying a fixed current. The difference between the resulting voltages is used to determine the values of the output resistance and capacitance. This technique, and its variations, has been used in other systems including the systems described in [8], [9], [10]. Despite the accuracy of the droop measurements, it cannot detect a change in the output impedance at the time of operation, i.e. when collecting image data, because it requires attaching the calibration resistors. Therefore, recalibrating the current sources requires a halt in the imaging process. The study presented in [11] intrinsically measures the output impedance of a single-source system by injecting current through a source and draining it via a ground node and comparing the injected current and the drained current. Another method is presented in [12] where authors build the admittance matrix of a single-source system and solve an estimation problem to infer the parasitic capacitances in the system.

The method presented in [2] which is used in this paper differs from other methods in the literature by providing a direct solution for measuring the output impedances of current sources in a multiple-source system while the imaging operation is ongoing.

III. Output Impedance Measurement

This section briefly discusses the proposed output impedance measurement technique. Additional details can be found in [2]. The technique depends on the linear independence of the standard patterns, and the relation between the sum of the injected current to the body and the current measured on the virtual ground node.

A. Zero-Sequence Pattern

The $N-1$ current patterns in the standard set of (1) are linearly independent and each current pattern sums to zero. A zero-sequence pattern, in which the currents on all electrodes are the same, is orthogonal to the basis of the standard patterns. This pattern is added as the Nth pattern to the system. In addition to being necessary for the output impedance calculation, this zero-sequence pattern can be used to detect a fault in the hardware of the system, such as a loose electrode [13].

B. Impedance Calculation

To measure the impedance, we can write the current measured on the virtual ground in terms of the sum of the currents applied through the electrodes as shown in (2)

$$\sum_{j=1}^{N} I_{L_j}^i = S^i \quad (2)$$

where i is indicator of the pattern number, j is the electrode number, N is the number of electrodes, $I_{L_j}^i$ is the current injected into the body through jth electrode on ith pattern, and S^i is the measured current on the virtual ground. We can then write $I_{L_j}^i$ in terms of the current applied by the source, and the current lost on the shunt impedance as shown in (3)

$$I_{L_j}^i = I_{S_j}^i - I_{Z_{o_j}}^i \implies I_{L_j}^i = I_{S_j}^i - V_j^i . G_{o_j} \quad (3)$$

where $I_{S_j}^i$ is the current of the jth source on ith pattern, $I_{Z_{o_j}}^i$ is the current lost on the output impedance of the same source and pattern, V_j^i is the voltage on the jth electrode for ith pattern, and G_{o_j} is the shunt admittance of the jth electrode.

By combining the expressions in (2) and (3), and writing them out for every pattern separately in a matrix form, we can simplify the whole expression to the form shown in (4).

$$\begin{bmatrix} G_{o_1} \\ \vdots \\ G_{o_N} \end{bmatrix} = \begin{bmatrix} -V_1^1 & \dots & -V_N^1 \\ \vdots & \ddots & \vdots \\ -V_1^N & \dots & -V_N^N \end{bmatrix}^{-1} * \begin{bmatrix} S^1 - \sum I_{S_j}^1 \\ \vdots \\ S^N - \sum I_{S_j}^N \end{bmatrix} \quad (4)$$

At the time of the operation, all the variables on the right-hand side, which are the electrode voltages, the virtual

ground current, and current amplitude of sources, are either measured or set by the user, meaning that the admittance values can be updated after collecting any frame of data with the overhead of just one pattern. i.e. the addition of the zero-sequence pattern that is not used to produce the EIT image.

IV. Experimental Setup

This section describes the practical setup of the system and the experiments.

A. EIT Hardware and Tank

The EIT system used in the project is a multiple source system with 32 current sources. Each source also acts as a voltmeter, measuring the voltage induced on its output. The operation frequency of the sources is 93 750 Hz and their signal-to-noise ratio is 96 dB when reading maximum voltage. All sources (current source and voltmeter) are calibrated to a common reference within a calibration system prior to the experiments. At the time of the imaging process, the calibration system acts as a virtual ground and measures the current present on a 33rd electrode connected to the virtual ground. The system can collect images with the speed of up to $\approx 30 \frac{frames}{s}$.

Data was taken using a saline-filled 30 cm diameter circular tank with one row of 32 2.54 cm $\times$ 2.54 cm stainless steel electrodes around its circumference. The tank is shown in Fig. 2. The cables connecting the sources to the electrodes are 2 m double-shielded cable with a DC-blocking capacitor at their end. The cable shields are grounded. A similar cable, without the DC-blocking capacitor is used for the virtual ground connection.

B. Adaptive Sources

The EIT system used in this paper utilizes adaptive current sources [3], [4]. These sources take the shunt impedance values (Z_o) as an input and monitor the induced voltage (V) on their output in real-time. They track the lost current on the shunt impedance by calculating $\frac{V}{Z_o}$ and adapt their current output to compensate this lost current, ideally making the current injected into the load exactly the same as the desired current. Since the performance of the adaptive compensation method is directly related to the accuracy of estimate of the shunt admittance, providing more accurate values for the admittance means that the compensation method will perform better.

C. Impedance Measurements

The shunt impedance of the current sources are first measured through open circuit measurements. Here, the cables are detached from the tank and spaced apart. Each source is activated with a 5 µA current and the induced voltages are measured. The known applied current and measured voltages are used to compute the open circuit (OC) impedance values. To minimize the effects of noise, each measurement is repeated 1000 times and the results are averaged.

Another set of output impedance values (Adaptive impedance) are measured using the proposed method in this paper. These measurements are made with the cables connected to the saline-filled tank and imaging data is being collected. At first, the sources utilize the OC output impedance values and they are later updated to the adaptive values.

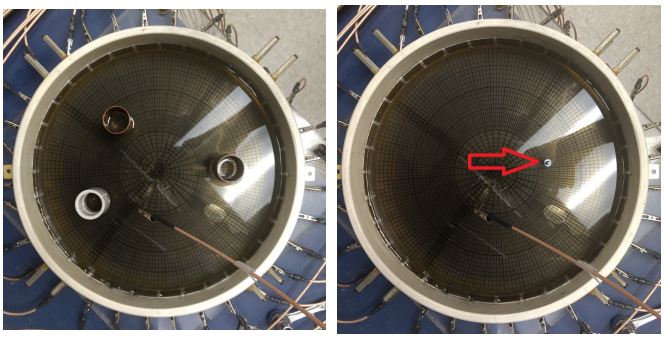

(a) (b)

Fig. 2: Two configurations of objects in saline tank: (a) three large objects for comparison of images, and (b) a small object for comparing other performance metrics.

The maximum amplitude of the applied current for each source is 200 µA for the standard patterns, while the amplitude of the zero-sequence current pattern for each source is 2 µA.

D. Experiments

Each of the experiments described in this section are done under both configurations - sources operating with the OC impedance and sources operating with the adaptive impedance and for each experiment the system collects 1000 frames of data.

At first, the image of the saline-filled tank with no targets is collected to be used as background image. At the next step, to ensure the validity of the data, data is collected with three targets placed in the tank as shown in Fig. 2a. Next, to show how the two configuration can capture information related to small changes in the body, more data is collected with a small conductive target in the tank as shown in Fig. 2b

E. Performance Metrics

The metrics that are used for comparison between the performance of the two methods are (i) the current passing through the virtual ground and (ii) two distinguishability criteria [14], norm distinguishability and power distinguishability.

The current on the Virtual ground of the system is an indicator of how effective the impedance measurements are. If the shunt impedance is measured with no error, the adaptive sources will properly compensate the lost current on them. If there is an error in the impedance measurement, there will be a mismatch on the compensated current and the lost current on the impedance. These mismatched currents are going to be summed up on the virtual ground, meaning that under ideal circumstances, there will be zero current on the virtual ground. In general, better estimates of the output

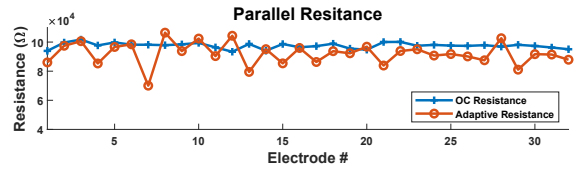

(a)

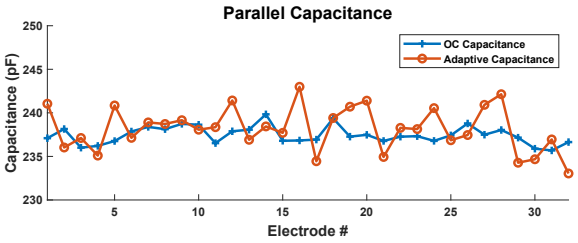

(b)

Fig. 3: Comparison of measured parallel impedance of each current source with OC measurements and the adaptive measurements divided to (a) parallel resistance, and (b) parallel capacitance.

impedance values results in smaller current passing through the virtual ground.

The other performance metrics are the norm and power distinguishability factors. These metrics provide a measure of the difference between one set of voltage measurements for one conductivity distribution, e.g. targets in the tank, and a second set of voltage measurements, e.g. no targets in the tank. The norm distinguishability factor takes the voltage difference of two measurements into account by calculating the expression in (5) where σ_0 and σ_1 are the two imaged conductivities, j is the current density, N is the number of electrodes, k is the number of pattern, I_n^k is the current on the nth electrode in kth pattern, and V_n^k are the induced voltages on the same electrode during the same pattern.

$$D^k_{\text{Norm}} = \sqrt{\frac{\sum_{n=1}^{N} |V_n^k(\sigma_1, j) - V_n^k(\sigma_0, j)|^2}{\sum_{n=1}^{N} |I_n^k|^2}} \tag{5}$$

The power distinguishability factor looks at the power difference between two measurements as shown in (6) where P is the power and is the real part of $I.V$.

$$D^k_{\text{Power}} = \frac{\sum_{n=1}^{N} |P_n^k(\sigma_1) - P_n^k(\sigma_0)|}{\sum_{n=1}^{N} |P_n^k(\sigma_0)|} \tag{6}$$

V. Results

This section, discusses the results of the experiments.

A. Impedance Measurements

The first step to demonstrate the feasibility of the proposed method is to validate impedance measurement values. The measured values for the impedance are shown in Fig. 3, where Fig. 3a shows the shunt resistance and Fig. 3b plots the shunt capacitance. In parallel they form the output impedance for each current source. Note that at the frequency of operation, the capacitance has a more significant impact

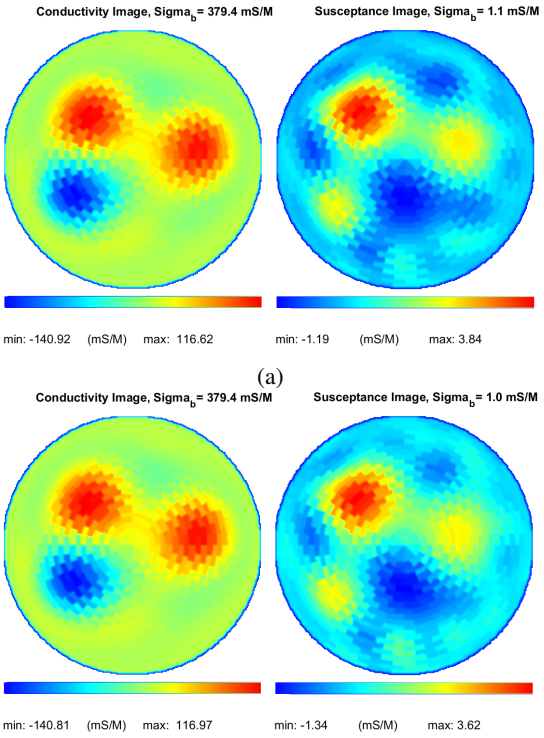

(a)

(b)

Fig. 4: Reconstructed Image of three targets in tank under (a) OC impedance, and (b) adaptive impedance configurations.

on the magnitude of the shunt output impedance. It can be seen that the OC and adaptive impedance are in the same range, yet the results of the two methods are not identical. It is likely that the adaptive results are more varied due to interaction between the output impedances associated with nearby electrodes. Current from one source can flow into the output impedance of another source through the conductive saline that connects the electrodes, though the algorithm will assign that current flow to the source output impedance.

B. Reconstructed Images

Reconstructed difference images for the case with multiple targets (Fig. 2a) is shown in Fig. 4. The images are created using the NOSER algorithm [15] and subtracting the saline only image from the target image. The left and right images are the conductivity and susceptibility, respectively. The two upper targets are copper pipes, with the one on the left having a thin layer of oxide that creates a capacitive component observable in the susceptibility image. The lower target is PVC pipe. The images are formed by averaging voltages from 1000 frames. Fig. 4a shows the result using the OC impedances and Fig. 4b show the result using the adaptive impedances. The sets of images are nearly identical.

C. Ground Current

The ground current under the two configurations of OC impedance and the Adaptive impedance is shown in Fig. 5. The results show that for all patterns of current, virtual ground current is lower when the sources are operating with

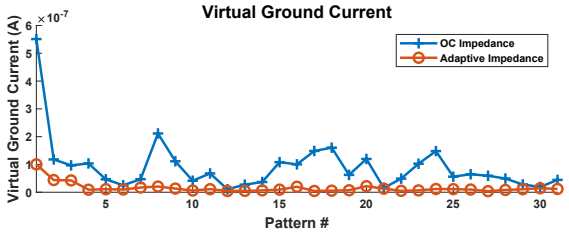

Fig. 5: Amplitude of mismatched current collected through the virtual ground under the two operation configurations of (i) OC impedance and (ii) adaptive impedance.

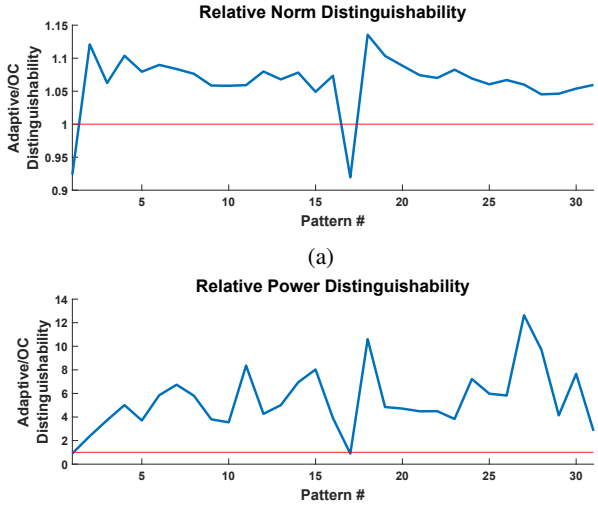

Fig. 6: Relative (a) norm distinguishability, and (b) power distinguishability of collected data.

the adaptive impedance as opposed to them operating with the OC impedance.

D. Distinguishability

The distinguishability measures for the small target of Fig. 2b were computed with adaptive and OC output impedances and their ratios are plotted in Fig. 6. The results show that in all but 2 current patterns - the ones for the lowest spatial frequency cosine and sine - the adaptive impedance configuration has higher norm distinguishability and power distinguishability compared to the OC impedance configuration. These higher distinguishabilities point to the adaptive output impedances providing somewhat improved performance.

VI. Conclusion and Future Work

In this paper, a technique to extract the output impedances for current sources in an EIT system while attached to a load is discussed and its effectiveness is shown through experimental evaluations. In addition to the practical advantage of not needing to disconnect the system from the load to find the output impedances, the results show improved the performance by reducing the current passing through the virtual ground and higher distinguishability with a small target. The ability to continuously update the shunt impedance values can be especially useful in cases where EIT systems are used for an extended period of time. This method can be enhanced in future through adding more realistic cable models, taking the effects of a non-perfect virtual ground into the equations, and considering the effects of quantization error on the digital hardware on the measured impedance.

References

[1] David S Holder. Electrical impedance tomography: methods, history and applications. CRC Press, 2004.

[2] Omid Rajabi Shishvan, Ahmed Abdelwahab, and Gary J Saulnier. Measuring current source output impedance in EIT systems while attached to a load. In 2020 42nd Annual International Conference of the IEEE Engineering in Medicine & Biology Society (EMBC), pages 1452–1456. IEEE, 2020.

[3] Gary J. Saunlier, Ahmed Abdelwahab, and Farial Nur Maysha. DSP-based adaptive current source for EIT applications. In 20th International Conference on Biomedical Applications of Electrical Impedance Tomography. EIT2019, 2019.

[4] Gary J Saulnier, Ahmed Abdelwahab, and Omid Rajabi Shishvan. DSP-based current source for electrical impedance tomography. Physiological measurement, 41(6):064002, 2020.

[5] Michelle M Mellenthin, Jennifer L Mueller, Erick Dario León Bueno de Camargo, Fernando Silva de Moura, Talles Batista Rattis Santos, Raul Gonzalez Lima, Sarah J Hamilton, Peter A Muller, and Melody Alsaker. The ACE1 electrical impedance tomography system for thoracic imaging. IEEE Transactions on Instrumentation and Measurement, 68(9):3137–3150, 2018.

[6] DG Gisser, D Isaacson, and JC Newell. Current topics in impedance imaging. Clinical Physics and Physiological Measurement, 8(4A):39, 1987.

[7] Raymond Douglas Cook, Gary J Saulnier, David G Gisser, John C Goble, JC Newell, and David Isaacson. ACT3: a high-speed, high-precision electrical impedance tomograph. IEEE Transactions on Biomedical Engineering, 41(8):713–722, 1994.

[8] Tong In Oh, Kyung Heon Lee, Sang Min Kim, Hwan Koo, Eung Je Woo, and David Holder. Calibration methods for a multi-channel multi-frequency EIT system. Physiological measurement, 28(10):1175, 2007.

[9] Hun Wi, Harsh Sohal, Alistair Lee McEwan, Eung Je Woo, and Tong In Oh. Multi-frequency electrical impedance tomography system with automatic self-calibration for long-term monitoring. IEEE transactions on biomedical circuits and systems, 8(1):119–128, 2013.

[10] Jeffrey M Ashe, David Shoudy, Gregory Boverman, James Sabatini, Tzu-Jen Kao, and Bruce C Amm. A high precision parallel current drive experimental EIT system. In 15th International Conference on Biomedical Applications of Electrical Impedance Tomography. EIT2014, 2014.

[11] Xuetao Shi, Weichen Li, Fusheng You, Xuyang Huo, Canhua Xu, Zhenyu Ji, Ruigang Liu, Benyuan Liu, Yandong Li, Feng Fu, et al. High-precision electrical impedance tomography data acquisition system for brain imaging. IEEE Sensors Journal, 18(14):5974–5984, 2018.

[12] Adriana Machado Malafaia da Mata, Bruno Furtado de Moura, Marcio Ferreira Martins, Francisco Hernán Sepúlveda Palma, and Rogério Ramos. Parasitic capacitances estimation of an electrical impedance tomography data acquisition system by Bayesian inference. Measurement, 174:108992, 2021.

[13] Gregory Boverman, David Isaacson, Jonathan C Newell, Gary J Saulnier, Tzu-Jen Kao, Bruce C Amm, Xin Wang, David M Davenport, David H Chong, Rakesh Sahni, et al. Efficient simultaneous reconstruction of time-varying images and electrode contact impedances in electrical impedance tomography. IEEE Transactions on Biomedical Engineering, 64(4):795–806, 2016.

[14] David Isaacson. Distinguishability of conductivities by electric current computed tomography. IEEE transactions on medical imaging, 5(2):91–95, 1986.

[15] Margaret Cheney, David Isaacson, Jonathan C Newell, S Simske, and J Goble. NOSER: An algorithm for solving the inverse conductivity problem. International Journal of Imaging systems and technology, 2(2):66–75, 1990.